



TITLE:

Angle-resolved photoemission spectroscopy of liquid water at 29.5 eV

AUTHOR(S):

Nishitani, Junichi; West, Christopher W.; Suzuki, Toshinori

CITATION:

Nishitani, Junichi ...[et al]. Angle-resolved photoemission spectroscopy of liquid water at 29.5 eV. Structural Dynamics 2017, 4(4): 044014.

ISSUE DATE:

2017-04-07

URL:

<http://hdl.handle.net/2433/225176>

RIGHT:

© Author(s) 2017. All article content, except where otherwise noted, is licensed under a Creative Commons Attribution (CC BY) license (<http://creativecommons.org/licenses/by/4.0/>).

Angle-resolved photoemission spectroscopy of liquid water at 29.5 eV

Junichi Nishitani, Christopher W. West, and Toshinori Suzuki

Citation: *Structural Dynamics* **4**, 044014 (2017); doi: 10.1063/1.4979857

View online: <http://dx.doi.org/10.1063/1.4979857>

View Table of Contents: <http://aca.scitation.org/toc/sdy/4/4>

Published by the *American Institute of Physics*

Articles you may be interested in

Full observation of ultrafast cascaded radiationless transitions from $S_2(\pi\pi^*)$ state of pyrazine using vacuum ultraviolet photoelectron imaging

The Journal of Chemical Physics **145**, 044306 (2016); 10.1063/1.4955296

Charge-transfer-to-solvent reactions from I^- to water, methanol, and ethanol studied by time-resolved photoelectron spectroscopy of liquids

The Journal of Chemical Physics **145**, 074502 (2016); 10.1063/1.4960385

Time-resolved photoelectron imaging with a femtosecond vacuum-ultraviolet light source: Dynamics in the \tilde{A}/\tilde{B} - and \tilde{F} -bands of SO_2

The Journal of Chemical Physics **146**, 084301 (2017); 10.1063/1.4976552

Photoelectron spectroscopy of aqueous solutions: Streaming potentials of NaX (X = Cl, Br, and I) solutions and electron binding energies of liquid water and X^-

The Journal of Chemical Physics **140**, 174506 (2014); 10.1063/1.4871877

Molecular couplings and energy exchange between DNA and water mapped by femtosecond infrared spectroscopy of backbone vibrations

Structural Dynamics **4**, 044015 (2017); 10.1063/1.4980075

SVD-aided pseudo principal-component analysis: A new method to speed up and improve determination of the optimum kinetic model from time-resolved data

Structural Dynamics **4**, 044013 (2017); 10.1063/1.4979854



Angle-resolved photoemission spectroscopy of liquid water at 29.5 eV

Junichi Nishitani, Christopher W. West, and Toshinori Suzuki^{a)}

*Department of Chemistry, Graduate School of Science, Kyoto University,
Kitashirakawa Oiwake-cho, Sakyo-Ku, Kyoto 606-8502, Japan*

(Received 24 February 2017; accepted 27 March 2017; published online 7 April 2017)

Angle-resolved photoemission spectroscopy of liquid water was performed using extreme ultraviolet radiation at 29.5 eV and a time-of-flight photoelectron spectrometer. SiC/Mg coated mirrors were employed to select the single-order 19th harmonic from laser high harmonics, which provided a constant photon flux for different laser polarizations. The instrument was tested by measuring photoemission anisotropy for rare gases and water molecules and applied to a microjet of an aqueous NaI solution. The solute concentration was adjusted to eliminate an electric field gradient around the microjet. The observed photoelectron spectra were analyzed considering contributions from liquid water, water vapor, and an isotropic background. The anisotropy parameters of the valence bands ($1b_1$, $3a_1$, and $1b_2$) of liquid water are considerably smaller than those of gaseous water, which is primarily attributed to electron scattering in liquid water. © 2017 Author(s). All article content, except where otherwise noted, is licensed under a Creative Commons Attribution (CC BY) license (<http://creativecommons.org/licenses/by/4.0/>). [<http://dx.doi.org/10.1063/1.4979857>]

I. INTRODUCTION

Ultrafast spectroscopy using femtosecond lasers has revolutionized the studies of chemical reaction dynamics in atomic time- and length-scales to open a new research area of *femtochemistry*.¹ Besides many other achievements, real-time observation of non-adiabatic dissociation of NaI by Zewail and coworkers is the landmark in this field.² As represented by this example, photochemical reactions ubiquitously involve non-adiabatic transitions among potential energy surfaces and branching into different reaction products. For elucidating such complex reaction dynamics, it is crucial to observe the entire wave packet motion from the Franck-Condon region to the final products. Time-resolved photoelectron spectroscopy (TRPES) enables such experiments,³ if a sufficiently short probe wavelength becomes available to induce ionization from all electronic states of the reactant, transient species, and the products. Such a pulsed light source should be operated at a high repetition rate (on the order of kHz to MHz) to accumulate the experimental data while limiting the number of photoelectrons generated per laser shot to avoid space charge effects. High harmonic generation (HHG) driven by a high repetition-rate laser is a promising tool for TRPES from this point of view.^{4–9}

HHG is induced by focusing a driving laser beam (typically 800 nm and 1 mJ/pulse) into rare gas.^{10–14} It creates a number of odd harmonics simultaneously,¹⁵ supporting an attosecond pulse (or train) in the time domain. However, photoelectron spectroscopy (PES) in the frequency domain requires an adequate energy resolution, so that the photon energy distribution should be narrowed by sacrificing the pulse duration.^{4–6,8,9,16,17} For this purpose, time-preserving or time-delay compensated monochromators^{18,19} are usually employed. These monochromators have excellent performances, while their designs are complex and care must be taken to maintain a constant photon flux and directional pointing of monochromatized radiation when

^{a)} Author to whom correspondence should be addressed. Electronic mail: suzuki@kuchem.kyoto-u.ac.jp



changing the laser polarization. Therefore, the present study employs SiC/Mg coated mirrors to select the 19th single-order harmonic to ensure a constant photon flux for different polarizations.

Photoelectron spectroscopy (PES) has been widely applied to solid and gas targets, while liquids have been scarcely studied with this method, because PES requires high vacuum conditions. Nonetheless, Delahay, Siegbahn, and their coworkers have, respectively, challenged ultra-violet (UV) and X-ray PES of liquids since the late 60s.^{20,21} Faubel introduced a liquid microjet technique in the late 80s, which has reduced the technical difficulty associated with the introduction of volatile liquids into high-vacuum.²² Since the late 90s, a series of soft X-ray PES studies have been performed by Winter, Faubel, and their coworkers using synchrotron radiation.²³ More recently, TRPES of liquids has started in 2010 for real-time study of solution chemistry,^{24–26} in which time and angle-resolved photoelectron spectroscopy (TARPES) has been demonstrated using femtosecond UV lasers.^{27,28} TRPES using extreme UV (EUV) and near infrared (800 nm) femtosecond (or attosecond) lasers has also been reported,^{4–9,29} while the only example of angle-resolved PES (ARPES) of liquid in the EUV range is by Abel and coworkers at 38.7 eV.^{9,30} Photoionization of liquid water is an important target for ARPES from the viewpoint of radiation chemistry and biology, because ionization of cell water, which constitutes more than 70% of the living cell, is the initial step of radiation damages to a cell induced by high-energy particles or electromagnetic radiation. As an initial step of our effort toward EUV-TARPES, we present here ARPES of liquid water using our EUV light source at 29.5 eV.

II. EXPERIMENTAL

A schematic diagram of our experimental apparatus is shown in Fig. 1. A part of the output (1 mJ) from a one-box Ti-sapphire regenerative amplifier (Coherent Astrella, 35 fs, 800 nm, FWHM 40 nm, 1 kHz, 6 mJ) is focused using a quartz lens ($f = 500$ mm) into Kr gas filled in a 3/8 in. Teflon tube with 6.35 mm inner diameter. The pressure in this tube could not be measured, while the Kr pressure in a 1/8 in. SUS tube connected to the Teflon tube was measured to be 70 Torr. The driving laser beam passes across the Teflon tube through two pinholes drilled by the laser beam itself. The beam waist of the driving laser in the tube was estimated to be 0.2 mm. The Teflon tube is in a vacuum chamber, and Kr gas leaking through the pinholes is pumped out by a turbo molecular pump (TMP). The high harmonics generated in the Kr gas and the remaining driving laser beam co-propagate and enter the optics chamber, in which the driving laser beam is attenuated by an Al filter (200 nm thickness) and the 19th order single-ordered harmonic is selected using a concave ($R = 1000$ mm) and a flat SiC/Mg mirror, which are specifically designed to selectively reflect the 19th harmonic. The diameter of EUV light at the sample was measured to be $40\ \mu\text{m}$ in FWHM using photoionization of the microjet of $25\ \mu\text{m}$ in diameter. The photon flux was estimated to be 2×10^6 photon/pulse at maximum using a calibrated EUV photodetector (Opto Diode Corp., AXUV100Al).

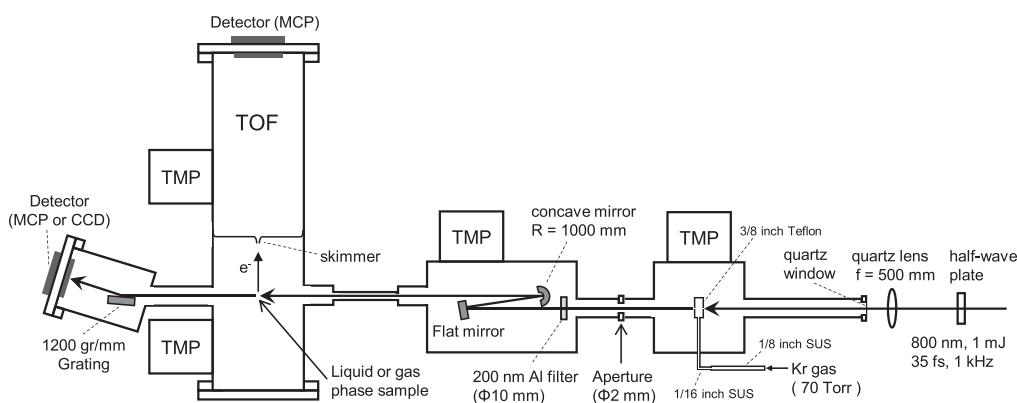


FIG. 1. Schematic diagram of our apparatus.

A liquid sample is pressurized using an HPLC gradient flow pump and degassed using a built-in degasser. The sample liquid is transferred from the degasser to a liquid-discharging nozzle using a temperature-controlled PEEK tube. The liquid is discharged into a photoelectron spectrometer through a fused silica capillary of 7 mm in length and 25 μm in inner diameter. The EUV laser beam crosses with the liquid microjet at 1 mm downstream from the capillary nozzle. Photoelectrons emitted from the microjet are sampled into a linear time-of-flight (TOF) analyzer using a 1-mm diameter Al entrance skimmer, coated with graphite, placed at 2 mm from the ionization point. The photoelectron spectrometer has been designed for X-ray PES, and it has two fine wire meshes after the entrance skimmer to decelerate incoming electrons. These meshes were electrically grounded in the experiments described below; however, they created weak background signals due to scattering. The detection solid angle is about 1 msr, determined by the radius (38 mm) of a microchannel plate detector and the flight distance (1200 mm). The electron signal from the microchannel plate is preamplified and counted using a multichannel scaler. The typical pressures in the photoionization chamber and the TOF analyzer are 1×10^{-4} and 1×10^{-6} Torr, respectively.

We examined the spectrum of the monochromatized EUV light in two ways: one is one-photon ionization of rare gases and the other is direct spectroscopic measurement of EUV light using a home-made EUV spectrometer. These measurements indicated that the intensity of the adjacent, the 17th and 21st, harmonics was less than 4% of the 19th, in agreement with the expected performance of the SiC/Mg mirrors. The linear polarization of the 19th harmonic is rotated using a half-wave plate for the driving laser (800 nm).^{31,32} Variation of the EUV photon flux was less than 4% when rotating polarization.

Figures 2(a) and 2(b), respectively, show the photoelectron spectra of Xe and Kr measured using P and S polarizations, in which P and S correspond to the linear polarization parallel and perpendicular to the electron detection axis. The lines observed in these spectra are considerably broader than their intrinsic linewidth previously measured by high-resolution photoemission spectroscopy, and the width (0.5 eV in FWHM) is primarily ascribed to the spectrum of EUV radiation. (The spectrum of EUV radiation varies with the Kr pressure and the driving laser intensity.) The fine structure splitting (0.665 eV) of Kr^+ is not well resolved, while that of Xe^+ (1.306 eV) is resolved with our resolution. The line shape is expressed by a Lorentzian. Figure 2(c) shows the photoelectron spectra of water molecules and the least squares fitting using exponentially modified Gaussians (EMGs); the functional form of EMG is described later. Three valence bands of $\text{X}(^2\text{B}_1)$, $\text{A}(^2\text{A}_1)$, and $\text{B}(^2\text{B}_2)$ are clearly seen. The vibrational structures of water bands are not well resolved owing to the large spectral width of our EUV light; however, the Franck-Condon envelopes agree with the literature. A small band at an electron binding energy (eBE) of 10 eV is the $1b_1$ band caused by the 21st harmonic; the observed spectra are shown against eBE calculated for the 19th harmonic, so that photoelectron bands caused by other harmonics are horizontally shifted by 3.1 eV. The weak continuous background signal seen in the water spectrum is due to electron scattering at the wire meshes described in Section II.

The photoemission anisotropy in a one-photon process is expressed by the following equation:

$$I(\theta) \propto 1 + \beta_2 P_2(\cos \theta), \quad (1)$$

where θ is the relative angle between the laser polarization and the electron detection angle and $P_2(x)$ is the second-order Legendre polynomial. β_2 is called an anisotropy parameter and is determined by the equation

$$\beta_2 = \frac{I(0) - I(90)}{\left(\frac{I(0)}{2}\right) + I(90)}, \quad (2)$$

where $I(0)$ and $I(90)$ are the intensities of the photoelectron bands measured using P and S polarizations, respectively. Table I lists the determined anisotropy parameters and literature values.

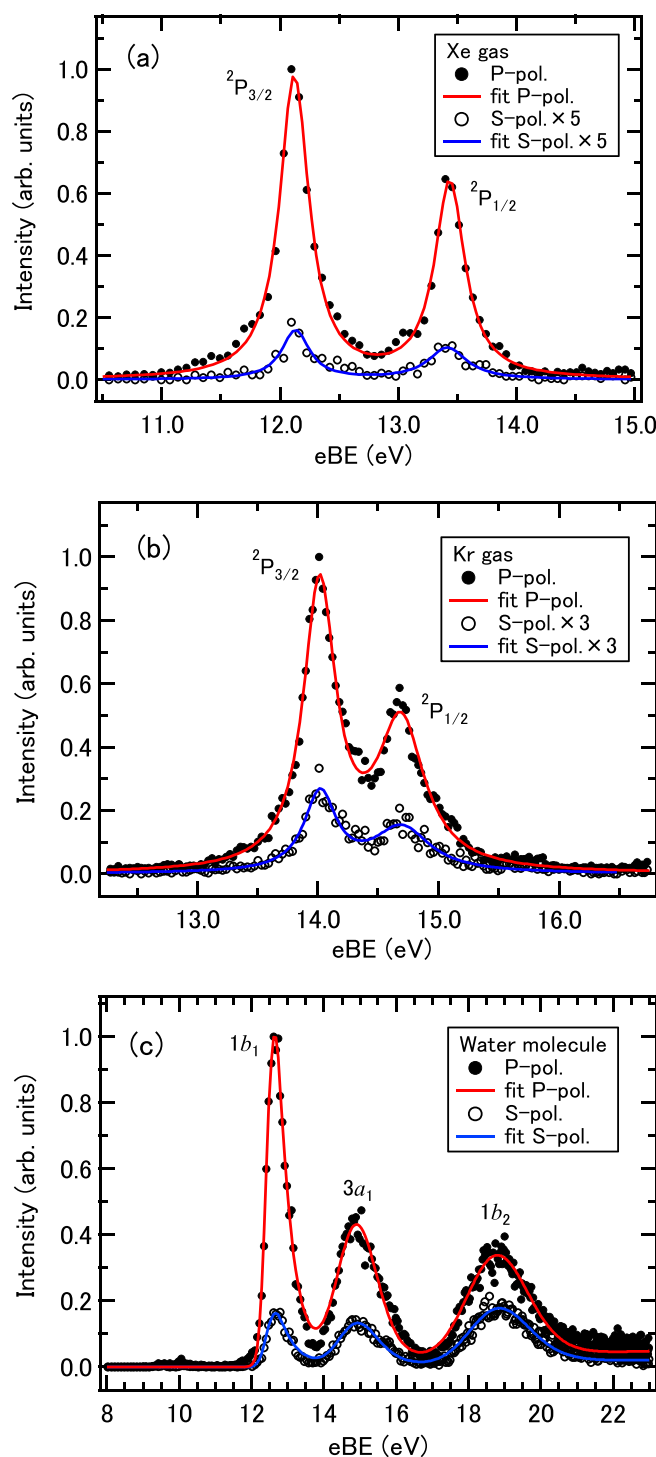


FIG. 2. Photoelectron spectra of (a) Xe, (b) Kr, and (c) water molecules measured using P and S polarizations of EUV light.

III. RESULTS AND DISCUSSION

Previously, Kurahashi *et al.* have shown that the surface potential of a liquid microjet is minimized at the NaX (X=halogen) concentration around 30 mM at the flow rate of 0.5 ml/min.³⁵ In the present study, we employed the same design of a liquid-discharging nozzle assembly, for

TABLE I. Photoemission anisotropy parameters (β_2) of rare gases and gaseous and liquid water.

	Photon energy (eV)	$^2P_{1/2}$	$^2P_{3/2}$		
Xe ⁺	26.86	1.86 ± 0.05	1.98 ± 0.04	Dehmer <i>et al.</i> ³³	
Xe ⁺	40.81	1.58 ± 0.03	1.28 ± 0.03	Dehmer <i>et al.</i> ³³	
Xe ⁺	29.5	1.82 ± 0.03	1.83 ± 0.03	This work	
Kr ⁺	26.86	1.50 ± 0.06	1.60 ± 0.05	Dehmer <i>et al.</i> ³³	
Kr ⁺	40.81	1.93 ± 0.06	1.90 ± 0.07	Dehmer <i>et al.</i> ³³	
Kr ⁺	29.5	1.49 ± 0.02	1.53 ± 0.02	This work	
		$1b_1$	$3a_1$	$1b_2$	
Gas water	30.0	1.31	0.93	0.49	Banna <i>et al.</i> ³⁴
Gas water	29.5	1.21 ± 0.05	0.86 ± 0.05	0.44 ± 0.06	This work
Gas water (Liquid) ^a	29.5	1.16 ± 0.06	0.79 ± 0.07 ^b	0.38 ± 0.07	This work
Liquid water	29.5	0.27 ± 0.07	0.24 ± 0.09	0.18 ± 0.06	This work

^aThe row of “Gas water (Liquid)” indicates anisotropy parameters of gaseous water extracted from the liquid water spectrum.

^bAs we assume in our analysis that both peaks in the $3a_1$ doublet are identical, we present a single anisotropy parameter for this peak.

which we confirmed, using completely different instruments, the same behavior of the surface potential as reported by Kurahashi *et al.*; they employed synchrotron radiation and a hemispherical electron energy analyzer, while we used laser high harmonics and a linear TOF analyzer. Figure 3 shows the photoelectron kinetic energy (PKE) associated with the $1b_1$ band of water molecules measured as a function of the distance of the ionization point from the liquid microjet. One can see that PKE is independent of the distance from the liquid microjet at the concentration of 30 mM, which implies that the electric potential of a liquid surface is equal to that of the entrance skimmer of the spectrometer. On the other hand, when using aqueous 10 and 100 mM solutions, PKE varies with the distance in opposite ways to each other. Thus, in order to avoid any influence of the electric field to photoemission anisotropy, we have employed the 30 mM solution in most of our experiments, while we used other concentrations for the purpose of comparison.

Figure 4(a) shows the photoelectron spectrum measured for the 30 mM solution using P and S polarizations. A background signal growing towards high eBE (low PKE) arises mainly from inelastic scattering of photoelectrons in solution, while some contributions of the secondary electrons generated by electron impact ionization and intermolecular Coulombic decay^{36,37} are also expected to contribute in the high eBE region. The valence bands appearing in the low eBE region are of liquid water and also water vapor evaporated from the jet surface. We performed least squares fitting of the spectra by assuming contributions from the liquid, vapor, and a broad background from inelastic scattering in water. The former two were expressed as a sum of EMGs

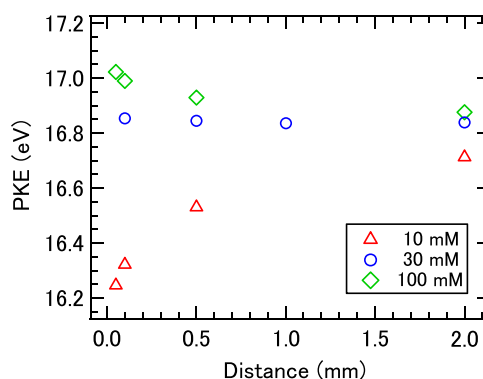


FIG. 3. Distance dependence of PKE measured for the $1b_1$ band of water molecules.

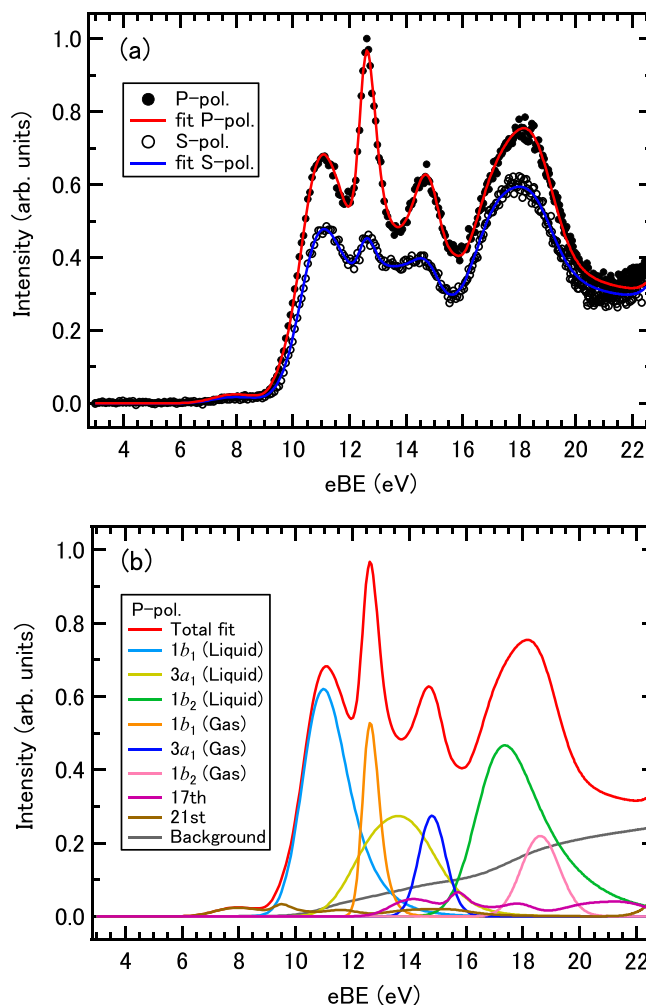


FIG. 4. (a) Photoelectron spectra measured for the 30 mM solution using P and S polarizations. (b) Each component obtained by the least squares fitting for the photoelectron spectrum measured using P polarization.

$$S_{Bands}(E; \mu_i, \sigma_i, \lambda_i) = \sum_i A_i \left(\frac{\lambda_i}{2} e^{\frac{\lambda_i}{2} (2(\mu_i + C_S) + \lambda_i \sigma_i^2 - 2E)} \operatorname{erfc} \left(\frac{(\mu_i + C_S) + \lambda_i \sigma_i^2 - E}{\sigma_i \sqrt{2}} \right) \right), \quad (3)$$

where S_{Bands} is the contribution to the fit from the photoelectron bands, E is the electron binding energy, i is the number of EMGs included in the fit, and A_i is the amplitude of the function. The parameters μ_i , σ_i and λ_i are the mean and variance of the Gaussian and the rate of the exponential, respectively. The values of μ_i for the $1b_1$, $3a_1$, and $1b_2$ bands were set to literature values. Finally, C_S is a constant to account for the PKE shift caused by the liquid surface potential, considered independently for both gas and liquid water; however, we restricted the bands of the same species (gas or liquid) to take the same C_S value to maintain the energy spacing of photoelectron bands. The relative intensities and energy separations of the vapor bands were fixed to the values determined for water molecules independently (Fig. 2(c)). However, the bandwidths were included in the fitting parameters, as these values show considerable variance in the vicinity of the liquid microjet (Fig. 6). The $3a_1$ band of liquid water was expressed using a doublet of identical EMGs with equal intensities, similar to the previous soft X-ray PES by Nishizawa *et al.*³⁸ There were also small signals from the neighboring harmonic orders weakly reflected by our SiC/Mg mirrors. The contributions from the 17th and 21st harmonics were treated similar to the 19th harmonic and so described as

$$S_{OHO}(E) = C_{17th}S_{Bands}(E; \mu_i + 3.1, \sigma_i, \lambda_i) + C_{21st}S_{Bands}(E; \mu_i - 3.1, \sigma_i, \lambda_i), \quad (4)$$

where C_{17th} and C_{21st} are constant factors of the 17th and 21st harmonic functions, respectively. The broad background component was estimated from the liquid water spectrum using an empirical formula based on the method described in Ref. 39. Briefly, the model assumes that the background is created by inelastic scattering and that the energy-loss function is independent of photoelectron kinetic energy. The number of scattered electrons at a certain energy is calculated in proportion to the number of unscattered electrons observed at lower eBE in the spectrum

$$I_{Background}(E) \propto \int_{E'=0}^E I_{Spectrum}(E') dE', \quad (5)$$

where $I_{Background}$ and $I_{Spectrum}$ are the intensities of the simulated background and the spectrum, respectively. It is noted here that if we simulate the background signal independently for P and S polarizations using Eq. (3), the anisotropy of the background becomes identical with that of unscattered electrons. This is unphysical, because the background electron signal generated by inelastic scattering in the liquid should exhibit lower anisotropy than the unscattered electron signals. Thus, we generated the common background signal function for P and S polarizations from the sum of liquid bands observed using these polarizations, which provided an entirely isotropic background signal

$$I_{Background}(E) = C_{BKG} \int_{E'=0}^E \left(S_P^{i=Liquid}(E') + S_S^{i=Liquid}(E') \right) dE', \quad (6)$$

where $S_P^{i=Liquid}$ and $S_S^{i=Liquid}$ are the intensities of the liquid bands observed in the P and S spectra, respectively, and C_{BKG} is a constant factor of the background function. Since the liquid water spectrum itself is determined by the least squares fitting, we performed iterative fitting to obtain consistent results between the estimated water spectrum and the broad background calculated from it. The photoelectron signals from Na^+ and I^- were sufficiently small to neglect. The function for the fit is then:

$$F(E) = S_{Bands}(E) + S_{OHO}(E) + I_{Background}(E). \quad (7)$$

The spectra for P and S polarizations were fitted simultaneously and the parameters μ_i , σ_i , and λ_i for the photoelectron bands were maintained between spectra. Each component obtained by the least squares fitting for P polarization is indicated in Fig. 4(b). The anisotropy parameter β_2 of each band was determined from the intensity ratio measured using P and S polarizations, as listed in Table I. The errors quoted with the anisotropy parameters were calculated from the experimental uncertainty derived from the energy resolution of the instrument and the variation in photon flux between P and S polarizations and the uncertainty in the fit. Owing to the surface reflection by the liquid microjet, the excitation probability is slightly different between P and S polarizations; however, its influence is negligible. Since the intensity due to inelastically scattered electrons continuously increases toward higher eBE (or lower PKE), ambiguity in the least squares fitting of the spectrum inevitably increases for the high eBE bands of $3a_1$ and $1b_2$ of liquid water. On the other hand, the $1b_1$ band of liquid water is almost isolated from other contributions, so that its β_2 value is most reliable. The β_2 value of the liquid $1b_1$ band is clearly smaller than the corresponding value of water molecules.

The spectral analysis described above indicates that the anisotropy parameters extracted for gaseous species in the vicinity of a microjet are very similar to, yet slightly smaller than those of water molecules. Thus, we have measured the photoemission anisotropy of water molecules more closely as a function of the distance from the liquid jet surface as shown in Fig. 5. The result indicates that the anisotropy diminishes as the ionization point approaches the microjet. Since this occurs similarly for different NaI concentrations, the reduction of the anisotropy

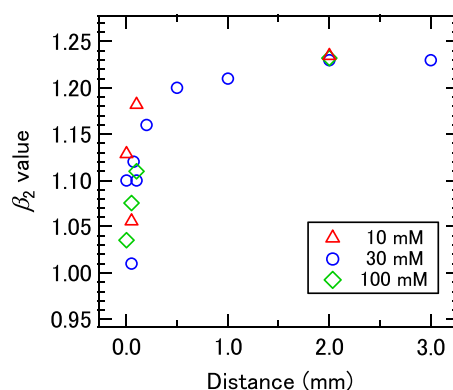


FIG. 5. Distance dependence of photoemission anisotropy of the $1b_1$ band of water molecules.

parameter is not ascribed to the liquid surface potential. There are at least three possible causes for the reduced photoemission anisotropy near the microjet. First, if too many photoelectrons are generated by an EUV laser pulse, the space charge reduces the anisotropy parameter. Secondly, if water clusters have high densities near the microjet, they would exhibit smaller anisotropy than water molecules. Finally, if electron-molecule scattering occurs in the evaporated gas, the anisotropy parameters diminish for all photoelectrons.

As for the first point, Figure 6 shows the observed photoelectron intensity of $1b_1$ band, the width of the fitted Gaussian, and the rate of exponential of the EMG as a function of the distance from the microjet. When the photoelectron intensity increases near the microjet, the width of the Gaussian and rate of exponential do change slightly. Although we examined the β_2 values by changing the EUV laser intensity, the intensity could be attenuated only by a factor of three to maintain a reasonable signal to noise ratio; within this intensity range, the β_2 values did not noticeably change. As for the second point, when a high-pressure liquid jet is discharged into vacuum, the internal pressure of the liquid abruptly diminishes and the interfacial wall is suddenly removed. This causes hydrodynamic instability, which might induce explosive evaporation of water molecules. Evaporated gas stagnates above the liquid surface and undergoes supersonic expansion, which lowers the gas pressure and possibly causes cluster formation. However, if cluster formation is the main cause for the reduction of anisotropy, it is not expected to depend so strongly on the distance. Finally, the momentum transfer cross-section between an electron and water molecule at the electron kinetic energy of 10 eV is about $8.5 \times 10^{-16} \text{ cm}^2$.⁴⁰ If we assume that the water vapor pressure above the liquid is saturated (the number density of $2.3 \times 10^{17} \text{ cm}^{-3}$ at 5 °C) and diminishes inversely proportional to the distance, the average number of collisions is estimated to be about 1. At the moment, the cause for the reduction of anisotropy near the jet surface is not totally clear. However, the space charge effect is the most likely cause. If this is the case, then the photoemission anisotropy parameters determined for both gaseous and liquid water by our experiment will in general be underestimated. For the $1b_1$ peak of gaseous water, which we might expect to show the largest reduction in the anisotropy parameter, this underestimation is less than 0.2. As the intrinsic anisotropy of the photoelectron feature decreases, the underestimation decreases proportionally.

Photoemission angular anisotropy provides valuable insights into an electronic character of the ionized state. Thürmer *et al.* have examined the photoemission angular distribution for soft X-ray O(1s) spectroscopy of liquid water using synchrotron radiation and demonstrated that the anisotropy is smaller than that of a water molecule.⁴¹ Hergenbahn and coworkers have measured photoemission anisotropy for neutral water clusters with the aggregation numbers (n) of 50–80 and attributed the diminished photoemission anisotropy to elastic scattering in the cluster.⁴² Nahon, Signorell, and their coworkers have employed a coincidence imaging spectrometer at SOLEIL to measure photoemission anisotropy as a function of electron kinetic energy for neutral water clusters up to $n=20$.⁴³ Their results are reproduced in Fig. 7. The anisotropy parameter diminishes in the range $n=1$ –6, while the value becomes almost invariant with n up

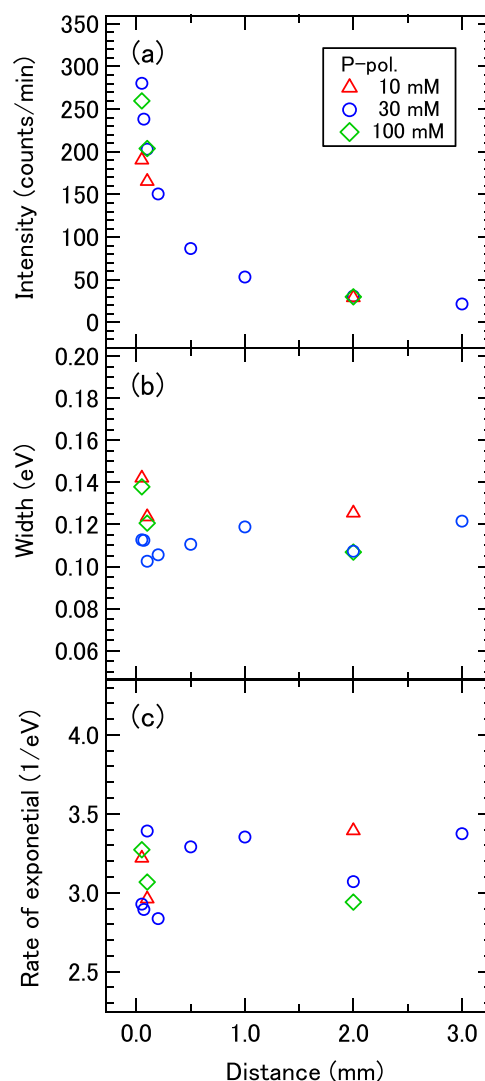


FIG. 6. Distance dependence of (a) photoelectron intensity of the $1b_1$ band of water molecules, (b) the width of the fitted Gaussian, and (c) the rate of exponential of the EMG.

to 20. The result indicated that the formation of hydrogen bonding network changes the character of ionized orbitals, especially $1b_1$ and $3a_1$ involved in hydrogen bonding, in small clusters. They have also predicted photoemission anisotropy of liquid water using the values of water clusters ($n = 1$ or 6) and Monte-Carlo simulations of the elastic and inelastic scattering of an electron in liquid water.⁴³ The green diamonds shown in Fig. 7 are β_2 values determined for water molecules, which almost agree with their experimental values,⁴² although our results are slightly smaller. The β_2 values determined for water molecules in the liquid water spectrum are indicated by blue diamonds. The experimental β_2 values for liquid water indicated by red diamonds are generally in reasonable agreement with the simulation using the water hexamer value, except that an ambiguity remains in our anisotropy parameters owing to possible space charge effects discussed above.

IV. CONCLUSION

We have constructed an EUV light source using SiC/Mg coated mirrors, which provided a constant photon flux for different polarizations. The performance of our instrument combining the EUV laser and a linear TOF photoelectron spectrometer was verified using photoemission

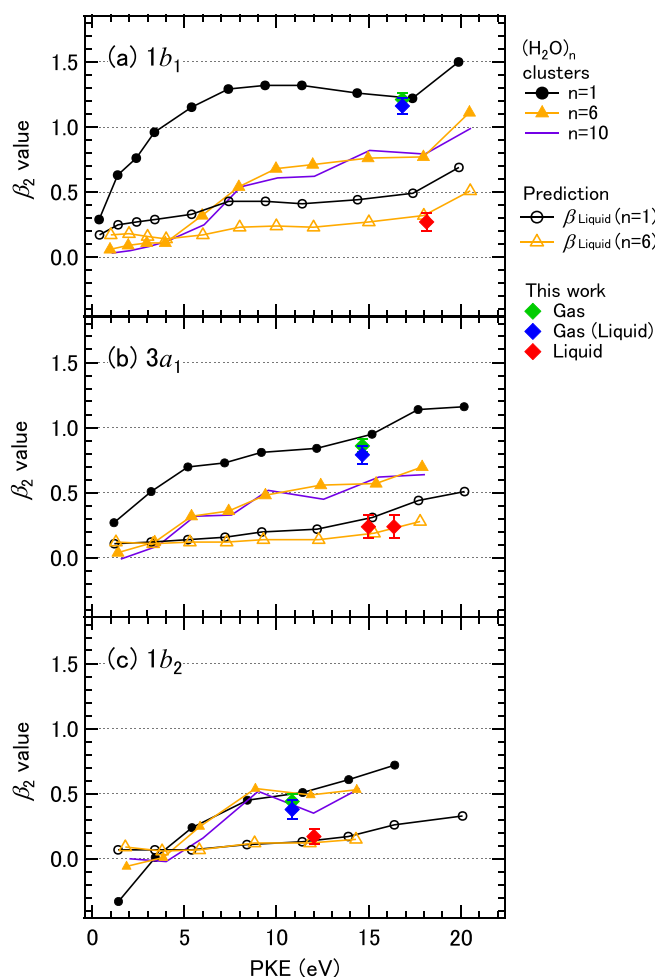


FIG. 7. Comparison of anisotropy parameters determined in this work and those obtained by Hartweg *et al.*⁴³ for (a) $1b_1$, (b) $3a_1$, and (c) $1b_2$ bands of water. Experimental values for H_2O monomer and $(H_2O)_n$ clusters and predicted values for liquid water were taken from Ref. 43. Open black circles indicate the prediction based on the β_2 values of monomer, and open orange triangles indicate the prediction based on cluster values ($n=6$). The experimental β_2 values determined for water molecules in this work are shown by green diamonds. Blue diamonds are β_2 values determined for water molecules in the liquid water spectrum. The β_2 values for liquid water are indicated by red diamonds. Two values are given for the liquid $3a_1$ band, as this band has been analyzed as a doublet.

spectroscopy of rare gases and water molecules. We measured the photoemission spectra of liquid water for P and S polarizations without an electric field gradient around a microjet by adjusting the electrolyte concentration. Careful analysis presented in this study illustrated various factors to be considered in the accurate determination of photoemission anisotropy for liquids. The photoemission anisotropy parameters of liquid water were considerably smaller than those of water molecules owing to inelastic scattering in the liquid, and they are in quantitative agreement with the theoretical prediction based on Monte-Carlo simulations.

ACKNOWLEDGMENTS

The authors are grateful to S. Thürmer for helpful discussions. We thank M. Hasumoto for his assistance in reflectivity measurements of SiC/Mg coated mirrors at UVSOR of the Institute for Molecular Science. S. Adachi and J. Itatani provided us with helpful advices on construction of the instrument. We thank R. Signorell for sending us the preprint of their paper. This work was supported by JSPS KEKENDHI Grant No. 15H05753. C. West was supported by a Research Fellowship for P16036 awarded by the Japan Society for the Promotion of Science.

- ¹A. H. Zewail, "Femtochemistry: Atomic-scale dynamics of the chemical bond," *J. Phys. Chem. A* **104**(24), 5660–5694 (2000).
- ²T. S. Rose, M. J. Rosker, and A. H. Zewail, "Femtosecond real-time probing of reactions. IV. The reactions of alkali halides," *J. Chem. Phys.* **91**(12), 7415–7436 (1989).
- ³T. Suzuki, "Time-resolved photoelectron spectroscopy of non-adiabatic electronic dynamics in gas and liquid phases," *Int. Rev. Phys. Chem.* **31**(2), 265–318 (2012).
- ⁴B. Frietsch, R. Carley, K. Dobrich, C. Gahl, M. Teichmann, O. Schwarzkopf, P. Wernet, and M. Weinelt, "A high-order harmonic generation apparatus for time- and angle-resolved photoelectron spectroscopy," *Rev. Sci. Instrum.* **84**(7), 075106 (2013).
- ⁵P. Wernet, J. Gaudin, K. Godehusen, O. Schwarzkopf, and W. Eberhardt, "Femtosecond time-resolved photoelectron spectroscopy with a vacuum-ultraviolet photon source based on laser high-order harmonic generation," *Rev. Sci. Instrum.* **82**(6), 063114 (2011).
- ⁶S. Plogmaker, J. A. Terschlusen, N. Krebs, M. Svanqvist, J. Forsberg, U. B. Cappel, J. E. Rubensson, H. Siegbahn, and J. Soderstrom, "HELIOS—A laboratory based on high-order harmonic generation of extreme ultraviolet photons for time-resolved spectroscopy," *Rev. Sci. Instrum.* **86**(12), 123107 (2015).
- ⁷C. Grazioli, C. Callegari, A. Ciavardini, M. Coreno, F. Frassetto, D. Gauthier, D. Golob, R. Ivanov, A. Kivimaki, B. Mahieu, B. Bucar, M. Merhar, P. Miotti, L. Poletto, E. Polo, B. Ressel, C. Spezzani, and G. De Ninno, "CITIUS: An infrared-extreme ultraviolet light source for fundamental and applied ultrafast science," *Rev. Sci. Instrum.* **85**(2), 023104 (2014).
- ⁸J. Ojeda, C. A. Arrell, J. Grilj, F. Frassetto, L. Mewes, H. Zhang, F. van Mourik, L. Poletto, and M. Chergui, "Harmonium: A pulse preserving source of monochromatic extreme ultraviolet (30–110 eV) radiation for ultrafast photoelectron spectroscopy of liquids," *Struct. Dyn.* **3**(2), 023602 (2016).
- ⁹O. Link, E. Lugovoy, K. Siefertmann, Y. Liu, M. Faubel, and B. Abel, "Ultrafast electronic spectroscopy for chemical analysis near liquid water interfaces: Concepts and applications," *Appl. Phys. A* **96**(1), 117–135 (2009).
- ¹⁰A. McPherson, G. Gibson, H. Jara, U. Johann, T. S. Luk, I. A. McIntyre, K. Boyer, and C. K. Rhodes, "Studies of multiphoton production of vacuum-ultraviolet radiation in the rare gases," *J. Opt. Soc. Am. B* **4**, 595–601 (1987).
- ¹¹A. L'Huillier, K. J. Schafer, and K. C. Kulander, "Theoretical aspects of intense field harmonic generation," *J. Phys. B: At. Mol. Opt. Phys.* **24**, 3315 (1991).
- ¹²P. B. Corkum, "Plasma perspective on strong field multiphoton ionization," *Phys. Rev. Lett.* **71**, 1994–1997 (1993).
- ¹³T. Brabec and F. Krausz, "Intense few-cycle laser fields: Frontiers of nonlinear optics," *Rev. Mod. Phys.* **72**, 545–591 (2000).
- ¹⁴J. Norin, J. Mauritsson, A. Johansson, M. K. Raarup, S. Buil, A. Persson, O. Dühr, M. B. Gaarde, K. J. Schafer, U. Keller, C.-G. Wahlström, and A. L'Huillier, "Time-frequency characterization of femtosecond extreme ultraviolet pulses," *Phys. Rev. Lett.* **88**, 193901 (2002).
- ¹⁵*Attosecond and XUV Physics: Ultrafast Dynamics and Spectroscopy*, edited by T. Schultz and M. Vrakking (Wiley VCH, 2014).
- ¹⁶I. Jordan, M. Huppert, M. A. Brown, J. A. van Bokhoven, and H. J. Wörner, "Photoelectron spectrometer for attosecond spectroscopy of liquids and gases," *Rev. Sci. Instrum.* **86**(12), 123905 (2015).
- ¹⁷A. von Conta, M. Huppert, and H. J. Wörner, "A table-top monochromator for tunable femtosecond XUV pulses generated in a semi-infinite gas cell: Experiment and simulations," *Rev. Sci. Instrum.* **87**(7), 073102 (2016).
- ¹⁸L. Poletto, P. Miotti, F. Frassetto, C. Spezzani, C. Grazioli, M. Coreno, B. Ressel, D. Gauthier, R. Ivanov, A. Ciavardini, M. de Simone, S. Stagira, and G. De Ninno, "Double-configuration grating monochromator for extreme-ultraviolet ultrafast pulses," *Appl. Opt.* **53**(26), 5879–5888 (2014).
- ¹⁹L. Poletto, P. Villorresi, E. Benedetti, F. Ferrari, S. Stagira, G. Sansone, and M. Nisoli, "Intense femtosecond extreme ultraviolet pulses by using a time-delay-compensated monochromator," *Opt. Lett.* **32**(19), 2897–2899 (2007).
- ²⁰H. Siegbahn, "Electron spectroscopy for chemical analysis of liquids and solutions," *J. Phys. Chem.* **89**(6), 897–909 (1985).
- ²¹P. Delahay, "Photoelectron emission spectroscopy of aqueous solutions," *Acc. Chem. Res.* **15**(2), 40–45 (1982).
- ²²M. Faubel, S. Schlemmer, and J. P. Toennies, "A molecular beam study of the evaporation of water from a liquid jet," *Z. Phys. D* **10**(2–3), 269–277 (1988).
- ²³B. Winter and M. Faubel, "Photoemission from liquid aqueous solutions," *Chem. Rev.* **106**(4), 1176–1211 (2006).
- ²⁴Y. Tang, H. Shen, K. Sekiguchi, N. Kurahashi, T. Mizuno, Y. I. Suzuki, and T. Suzuki, "Direct measurement of vertical binding energy of a hydrated electron," *Phys. Chem. Chem. Phys.* **12**(15), 3653–3655 (2010).
- ²⁵A. Lübcke, F. Buchner, N. Heine, I. V. Hertel, and T. Schultz, "Time-resolved photoelectron spectroscopy of solvated electrons in aqueous NaI solution," *Phys. Chem. Chem. Phys.* **12**(43), 14629–14634 (2010).
- ²⁶A. T. Shreve, T. A. Yen, and D. M. Neumark, "Photoelectron spectroscopy of hydrated electrons," *Chem. Phys. Lett.* **493**(4–6), 216–219 (2010).
- ²⁷Y. Yamamoto, Y. I. Suzuki, G. Tomasello, T. Horio, S. Karashima, R. Mitric, and T. Suzuki, "Time- and angle-resolved photoemission spectroscopy of hydrated electrons near a liquid water surface," *Phys. Rev. Lett.* **112**(18), 187603 (2014).
- ²⁸S. Karashima, Y. Yamamoto, and T. Suzuki, "Resolving nonadiabatic dynamics of hydrated electrons using ultrafast photoemission anisotropy," *Phys. Rev. Lett.* **116**(13), 137601 (2016).
- ²⁹K. R. Siefertmann, Y. X. Liu, E. Lugovoy, O. Link, M. Faubel, U. Buck, B. Winter, and B. Abel, "Binding energies, lifetimes and implications of bulk and interface solvated electrons in water," *Nat. Chem.* **2**(4), 274–279 (2010).
- ³⁰M. Faubel, K. R. Siefertmann, Y. Liu, and B. Abel, "Ultrafast soft x-ray photoelectron spectroscopy at liquid water microjets," *Acc. Chem. Res.* **45**(1), 120–130 (2012).
- ³¹D. Schulze, M. Dorr, G. Sommerer, J. Ludwig, P. V. Nickles, T. Schlegel, W. Sandner, M. Drescher, U. Kleineberg, and U. Heinzmann, "Polarization of the 61st harmonic from 1053-nm laser radiation in neon," *Phys. Rev. A* **57**(4), 3003–3007 (1998).
- ³²P. Antoine, A. L'Huillier, M. Lewenstein, P. Salieres, and B. Carre, "Theory of high-order harmonic generation by an elliptically polarized laser field," *Phys. Rev. A* **53**(3), 1725–1745 (1996).

- ³³J. L. Dehmer, W. A. Chupka, J. Berkowitz, and W. T. Jivry, “Wavelength dependence of the photoelectron angular distributions of the rare gases,” *Phys. Rev. A* **12**, 1966–1973 (1975).
- ³⁴M. S. Banna, B. H. McQuaide, R. Malutzki, and V. Schmidt, “The photoelectron spectrum of water in the 30 to 140 eV photon energy range,” *J. Chem. Phys.* **84**, 4739–4744 (1986).
- ³⁵N. Kurahashi, S. Karashima, Y. Tang, T. Horio, B. Abulimti, Y. Suzuki, Y. Ogi, M. Oura, and T. Suzuki, “Photoelectron spectroscopy of aqueous solutions: Streaming potentials of NaX (X = Cl, Br, and I) solutions and electron binding energies of liquid water and X[−],” *J. Chem. Phys.* **140**, 174506 (2014).
- ³⁶T. Jahnke, H. Sann, T. Havermeier, K. Kreidi, C. Stuck, M. Meckel, M. Schöffler, N. Neumann, R. Wallauer, S. Voss, A. Czasch, O. Jagutzki, A. Malakzadeh, F. Afaneh, Th. Weber, H. Schmidt-Böcking, and R. Dörner, “Ultrafast energy transfer between water molecules,” *Nat. Phys.* **6**, 139–142 (2010).
- ³⁷M. Mucke, M. Braune, S. Barth, M. Förstel, T. Lischke, V. Ulrich, T. Arion, U. Becker, A. Bradshaw, and U. Hergenhahn, “A hitherto unrecognized source of low-energy electrons in water,” *Nat. Phys.* **6**, 143–146 (2010).
- ³⁸K. Nishizawa, N. Kurahashi, K. Sekiguchi, T. Mizuno, Y. Ogi, T. Horio, M. Oura, N. Kosugi, and T. Suzuki, “High-resolution soft X-ray photoelectron spectroscopy of liquid water,” *Phys. Chem. Chem. Phys.* **13**, 413–417 (2011).
- ³⁹X. Li, Z. Zhang, and V. E. Henrich, “Inelastic electron background function for ultraviolet photoelectron spectra,” *J. Electron Spectrosc. Relat. Phenom.* **63**, 253–265 (1993).
- ⁴⁰Y. Itikawa and N. Mason, “Cross sections for electron collisions with water molecules,” *J. Phys. Chem. Ref. Data* **34**, 1–22 (2005).
- ⁴¹S. Thürmer, R. Seidel, M. Faubel, W. Eberhardt, J. C. Hemminger, S. E. Bradforth, and B. Winter, “Photoelectron angular distributions from liquid water: Effects of electron scattering,” *Phys. Rev. Lett.* **111**(17), 173005 (2013).
- ⁴²C. F. Zhang, T. Andersson, M. Forstel, M. Mucke, T. Arion, M. Tchapyguine, O. Bjorneholm, and U. Hergenhahn, “The photoelectron angular distribution of water clusters,” *J. Chem. Phys.* **138**(23), 234306 (2013).
- ⁴³S. Hartweg, B. L. Yoder, G. A. Garcia, L. Nahon, and R. Signorell, “Size-resolved photoelectron anisotropy of gas phase water clusters and predictions for liquid water,” *Phys. Rev. Lett.* **118**, 103402 (2017).